Organic & Biomolecular Chemistry

ROYAL SOCIETY OF CHEMISTRY

PAPER

View Article Online
View Journal

Cite this: DOI: 10.1039/d2ob00709f

A benzothiazole-based dual reaction site fluorescent probe for the selective detection of hydrazine in water and live cells†

Anwesha Maiti,[a] Saikat Kumar Manna,[b] Satyajit Halder,[c] Moumi Mandal,[a] Anirban Karak,[a] Dipanjan Banik,[a] Kuladip Jana[c] and Ajit Kumar Mahapatra *[a]

Received 15th April 2022,
Accepted 23rd May 2022

DOI: 10.1039/d2ob00709f

rsc.li/obc

As hydrazine is an environmental pollutant and highly toxic to living organisms, selective and rapid detection is highly needed for the benefit of living organisms as well as the environment. Here, we first introduced a novel benzothiazole conjugated methyldicyanovinyl coumarin probe **BTC**, with dual recognition sites for hydrazine detection. The incorporation of the methyldicyanovinyl group into the benzocoumarin fluorophore increased the electrophilicity of the lactone ring of the probe **BTC** facilitating the nucleophilic attack of hydrazine and rapid (within 1 min, low detection limit = 1.7 nM) turn-on sky blue fluorescence with 700-fold fluorescence intensity enhancement was observed *via* hydrazine-induced lactone ring-opening followed by selective cleavage of the dicyanovinyl group. According to the literature, dicyanovinyl group assisted lactone ring opening has revealed the possibility of hydrazine recognition with a large Stokes shift (140 nm) and a high fluorescence quantum yield (0.67). Here, the DFT study and practical applications of the probe **BTC** in different water samples have been presented. The probe **BTC** was also successfully applied for the detection of hydrazine in the vapor phase using paper strips and in live MDA-MB 231 cells.

Introduction

Hydrazine is a highly reactive reducing agent and important chemical reagent that has wide practical applications in many fields, *i.e.*, the chemical and pharmaceutical industries, synthesis of pesticides, plastics, polymers, dyes and textiles, chemotherapeutics, photographic developers, *etc*.[1–5] Due to the high enthalpy of combustion, hydrazine is also applied in missiles and various rocket fuels as a propellant.[6] Hydrazine is highly toxic and poisonous to humans and living organisms.[7] Toxicity studies have shown that hydrazine is easily absorbed during usage, transport, and disposal. Prolonged exposure to hydrazine may cause severe lung, kidney and liver damage and may affect the central nervous system also.[8,9] The United States Environment Protection Agency (EPA) has listed hydrazine as a human carcinogenic agent with a low threshold limit value of 10 ppb or 0.312 μM.[10] Hence, it is high time to design suitable hydrazine-specific chemodosimeters for human and environmental safety.

Various analytical methods for hydrazine detection, including mass spectrometry,[11] chromatography,[12] titrimetry,[13] surface-enhanced Raman spectroscopy,[14] and electrochemical methods,[15] have been developed to date. But among several techniques, the fluorescence method-based approach is highly attractive because of its lower cost, less time consumption, higher selectivity, and sensitivity.[16] In the literature, most of the reported fluorescent chemodosimeters for hydrazine detection have been designed based on the cleavage of the acetoxy group,[17–22] deprotection of the phthalimide moiety,[23–27] nucleophilic addition–elimination reaction on keto ester,[28–31] pyrazole ring formation,[32–35] chemical displacement of the active methylene group to the corresponding hydrazone derivative,[36–40] *etc*. Sun *et al.* have synthesized a phenothiazine conjugated dicyanomalonitrile fluorescent turn-on probe for hydrazine detection.[41] Li *et al.* have reported a cyanoacetate-naphthalene compound as a fluorescent turn-on probe for hydrazine.[42] Fan *et al.* have developed a ratiometric dicyano derivative for hydrazine detection.[43] But in all cases, these probes suffer from low selectivity, higher detection limit value (micromolar region), lower Stokes shift, and lower change in

[a]*Department of Chemistry, Indian Institute of Engineering Science and Technology, Shibpur, Howrah-711103, West Bengal, India.*
E-mail: akmahapatra@chem.iiests.ac.in
[b]*Department of Chemistry, Haldia Government College, Debhog, Haldia, Purba Medinipur-721657, West Bengal, India*
[c]*Division of Molecular Medicine, Bose Institute, P 1/12, CIT Scheme VIIM, Kolkata-700054, India*

† Electronic supplementary information (ESI) available. See DOI: **https://doi.org/10.1039/d2ob00709f**

the fluorescence intensity signal. Hence, the design of chemodosimeters with suitable reactive sites, high selectivity, good water solubility, large Stokes shift, and large fluorescence enhancement is challenging to researchers nowadays.

Here, we have reported a new type of fluorescent "turn-on" probe **BTC** with a dual recognition site based on both hydrazine-induced lactone ring-opening reaction and dicyanovinyl group cleavage (Scheme 1). Due to the hydrazine-induced lactone ring-opening reaction and dicyanovinyl group cleavage, a strong enhancement in the fluorescence intensity signal with a large Stokes shift was observed. This was probably due to the presence of a methyl dicyanovinyl group on the lactone moiety of the probe **BTC**, which not only increased the electrophilicity of the lactone ring to attack nucleophilic hydrazine, but also, after the ring-opening reaction, led to a large Stokes shift (140 nm) due to the increase in the conjugated chain length by virtue of cleavage of the dicyanovinyl group to the hydrazone derivative. Moreover, the **BTC-A** adduct (Scheme 5) showed a solvatochromism effect by integrating PET (photoinduced electron transfer) with ICT (intramolecular charge transfer) and ESIPT (excited-state intramolecular proton transfer) processes operating in different solvent systems, as a result of which a strong fluorescence signal was observed.[44–46] The probe **BTC** has been successfully applied to detect hydrazine in the vapor state, real water samples, and MDA-MB 231 cells.

Experimental section

Materials and methods

All reagents and solvents were purchased from commercial suppliers and were used without further purification. The products were purified by column chromatography using silica gel (60–120 mesh). Thin layer chromatography was performed on silica gel 60 F254 plates. UV-visible and fluorescence spectra were recorded using JASCO V530 and PerkinElmer LS55 spectrofluorometers, respectively. ^{1}H NMR and ^{13}C NMR spectra were recorded using a Bruker 400 MHz instrument. $CDCl_3$ was used as a solvent for recording NMR spectra. ESI-MS spectra were recorded using a PerkinElmer 2400 series CHNS/O Analyzer.

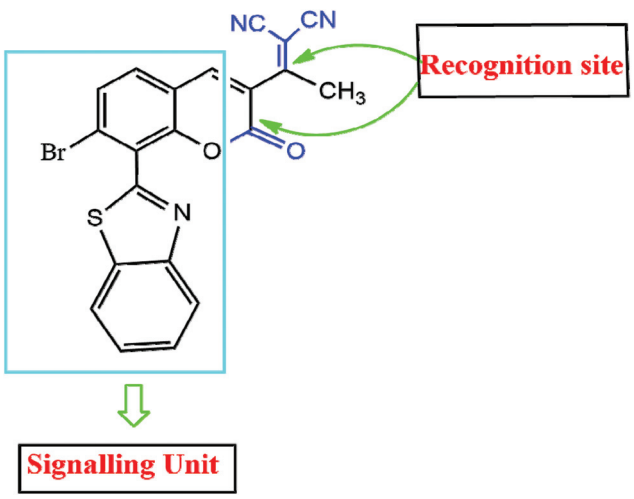

Scheme 1 Structure of chemodosimeter **BTC**.

UV-vis absorption and fluorescence studies

For UV-vis and fluorescence titration experiments, the test solutions of the probe **BTC** ($c = 4 \times 10^{-5}$ M) and analytes containing guest cations, anions and primary amines ($c = 4 \times 10^{-4}$ M) were prepared in DMSO–H_2O (7 : 3, v/v) solution (10 mM HEPES buffer, pH 7.4) from the stock solution by an appropriate dilution method.

^{1}H NMR titration

The ^{1}H NMR titration experiment was carried out by adding different equivalents of hydrazine to the solution of the probe **BTC** dissolved in DMSO-d_6.

Preparation of test strips

A series of test strips of different concentrations (1.0×10^{-5} M, 1.0×10^{-4} M, 1.0×10^{-3} M, 1.0×10^{-2} M, 4.0×10^{-2} M) were prepared by immersing filter paper in the (DMSO–H_2O = 7 : 3 v/v, pH = 7.4) solutions of **BTC** (1.0×10^{-5} M) and then drying in air. The test strips were covered on the top of jars containing different concentrations of hydrazine solution (blank, 0.1%, 0.5%, 1%, 5%, 10%, 20%, 25%, 30%, 40% and 50% in water) for 30 min at room temperature before they were ready for observation.

Cell line study

In the present study, the human breast cancer cell line MDA-MB 231 and human normal lung fibroblast cell line WI-38 were procured from NCCS, Pune, India. All the cell lines were cultured in a T25 flask with DMEM supplemented with 10% FBS, 2 mM L-glutamine, non-essential amino acids, 1 mM sodium pyruvate, penicillin, 100 mg L^{-1} streptomycin, and 50 mg L^{-1} gentamycin in a 37 °C humidified incubator containing 5% CO_2.

Cytotoxicity assay

A MTT cell proliferation assay[47] was performed to assess the cytotoxic effect of the probe **BTC** in both the cancer cell line MDA-MB-231 and the normal cell line WI-38. In brief, cells were first seeded in 96-well plates at a concentration of 1×10^4 cells per well for 24 h and exposed to different working concentrations of the probe **BTC** in DMSO (0–80 μM) for 24 h. After incubation, the cells were washed with 1× PBS and MTT solution (0.5 mg ml^{-1}) was added to each well and incubated for 4 h. The resulting formazan crystals were dissolved in DMSO and the absorbance was measured at 570 nm using a microplate reader. Cell viability was expressed as a percentage of the control experimental setup.

Fluorescence imaging

To envision the fluorescence ability of the probe **BTC** in the presence of hydrazine, fluorescence imaging was performed in the cell line MDA-MB 231. Briefly, cells were grown in coverslips for 24 h in a 37 °C humidified incubator containing 5% CO_2 and then either mock-treated or treated with 15 μM of the

probe **BTC** in the presence or absence of 10 μM hydrazine separately and incubated for 30 min in the dark at 37 °C. The cells were washed with 1× PBS and then they were mounted on a glass slide and observed under a fluorescence microscope (Olympus) using a DAPI filter.[48]

Synthesis of compounds 2–5

Compounds **2–5** were synthesized according to the literature method.[49–51]

Synthesis and characterization of the probe BTC

Compound **5** (250 mg, 0.62 mmol), malonitrile (82.7 mg, 1.24 mmol) and NH_4OAC (118.0 mg, 1.5 mmol) were dissolved in AcOH and refluxed in toluene (6 ml) for 12 hours. After refluxing for 12 hours, the mixture was poured into deionized water and extracted with ethyl acetate (30 ml × 3). The collected organic layer was washed with water, filtered and dried over $MgSO_4$. The residue was purified by column chromatography (petroleum ether/ethyl acetate 8 : 1) to give the desired product **BTC** as a yellow solid (100 mg, yield 35%) (Scheme 2).

BTC. ^{1}H NMR (400 MHz, $CDCl_3$): δ 2.20 (s, 3H), 6.40 (s, 1H), 7.48 (t, J = 16.0 Hz, 1H), 7.60 (t, J = 16.0 Hz, 1H), 7.89 (d, J = 12.0 Hz, 1H), 8.18 (d, J = 8.0 Hz, 1H), 8.04 (d, J = 8.0 Hz, 1H), 8.53 (d, J = 20.0 Hz, 1H).

^{13}C NMR (100 MHz, DMSO-d_6): δ 30.57 (1C), 109.45 (1C), 117.96 (1C), 120.23 (2C), 121.74 (2C), 123.57 (2C), 125.33 (1C), 125.99 (1C),

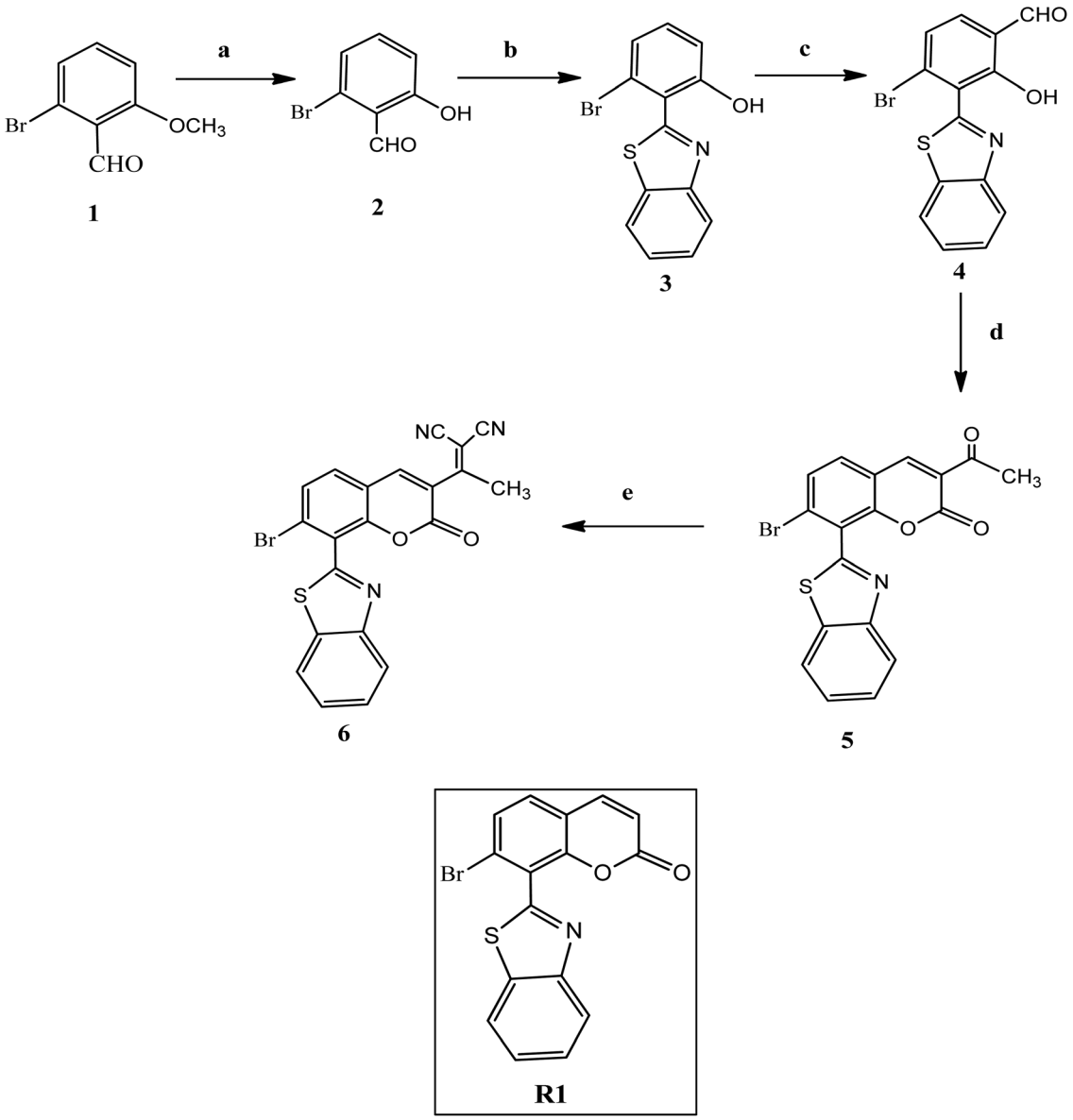

Scheme 2 Synthesis of **BTC**, *reagents and conditions*: (a) BBr_3, CH_2Cl_2, r.t., 5 hours; (b) 2-aminothiophenol, $KHSO_4$ (cat), EtOH, reflux at 60–65 °C, 5 hours; (c) trifluoroacetic acid/hexamine, reflux at 80 °C, 28 hours; (d) ethyl acetoacetate, EtOH, piperidine, reflux overnight at 70 °C; (e) malonitrile, AcOH, NH_4OAC, toluene, reflux at 80 °C, 12 hours.

126.76 (1C), 133.93 (1C), 135.41 (1C), 136.41 (1C), 146.22 (1C), 151.08 (1C), 151.99 (1C), 158.07 (1C), 158.45 (1C), 182.69 (1C).

HRMS (ESI): *m*/*z*, calc. for $C_{21}H_{10}BrN_3O_2S^+$ $(M + H)^+$ 447.9750; found 447.9752.

Results and discussion

Synthesis

The probe **BTC** was synthesized in five steps. The synthetic route of the probe **BTC** is described in Scheme 2.

The probe **BTC** was synthesized in five steps starting from the precursor 2-bromo-6-methoxy benzaldehyde. (a) The reaction of 2-bromo-6-methoxy benzaldehyde **1** with boron tribromide in CH_2Cl_2 medium resulted in the formation of 2-bromo-6-hydroxy benzaldehyde (**2**). (b) 2-Bromo-6-hydroxybenzaldehyde (**2**), upon condensation with 2-amino thiophenol using $KHSO_4$ as a catalyst in ethanol medium and refluxing conditions at 60–65 °C for 5 hours, gave the product 2-bromo-6-hydroxybenzothiazole coumarin (**3**). (c) 2-Bromo-6-hydroxybenzothiazole coumarin (**3**), on reaction with trifluoroacetic acid and hexamine under refluxing conditions at 80 °C overnight gave the product 2-bromo benzothiazole coumarin hydroxy aldehyde (**4**). (d) The product **4** underwent a condensation reaction with ethyl acetoacetate and piperidine in ethanol medium under refluxing conditions at 70 °C overnight generating the product **5**. (e) The product **5**, on reaction with malononitrile and NH_4OAC dissolved in AcOH under refluxing conditions at 80 °C in toluene for 12 hours, gave the final probe **BTC**. The structure of the probe **BTC** was characterized by HRMS, ^{1}H NMR, and ^{13}C NMR (Fig. S1–S3, ESI†)

UV-vis study

The UV-vis spectrum of the probe **BTC** showed two maximum absorptions at 306 nm and 369 nm respectively in aq. DMSO (DMSO/H_2O = 7 : 3 v/v, 10 mM HEPES buffer, pH = 7.4) (Fig. 1a). The peak at 306 nm corresponds to the π–π* transition and that at 369 nm corresponds to the n–π* transition respectively. With increasing hydrazine concentration, the absorption peaks at 306 nm gradually decreased and two peaks appeared at 423 nm and 517 nm respectively. The peaks at 423 nm and 517 nm correspond to both hydrazine-induced dicyanovinyl group cleavage and lactone ring-opening reaction.

In the probe **BTC**, the dicyanovinyl group was somehow tilted towards the fluorophore which became planar after the hydrazine induced lactone ring-opening reaction. As a result, the conjugated chain length increased and a bathochromic shift occurred. Simultaneously, a well-defined isosbestic point was noted at 377 nm, indicating the formation of the **BTC-A** adduct (Scheme 5) as well as a clean chemical transformation. This result indicated the formation of a new species. The same was recognized by the naked-eye color change from light yellow to reddish brown, which allowed the direct visual detection of hydrazine. The appearance of the reddish-brown color (λ_{max} = 517 nm) and the large bathochromic shift (211 nm) in the absorption spectrum suggested that hydrazine caused the lactone ring-opening of the probe **BTC**, which was thought to be responsible for this color change. Moreover, with an increase in the hydrazine concentration, the absorbance of the probe decreased as the area of absorption decreased due to lactone ring-opening (Fig. 1b).

Fluorescence study

To examine the enhanced fluorescence response of **BTC** in aqueous DMSO (DMSO/H_2O = 7 : 3 v/v, 10 mM HEPES buffer, pH = 7.4), the probe solution was titrated spectrofluorometrically against an increasing concentration of N_2H_4. As shown in Fig. 2a, the free probe displayed an emission peak with the

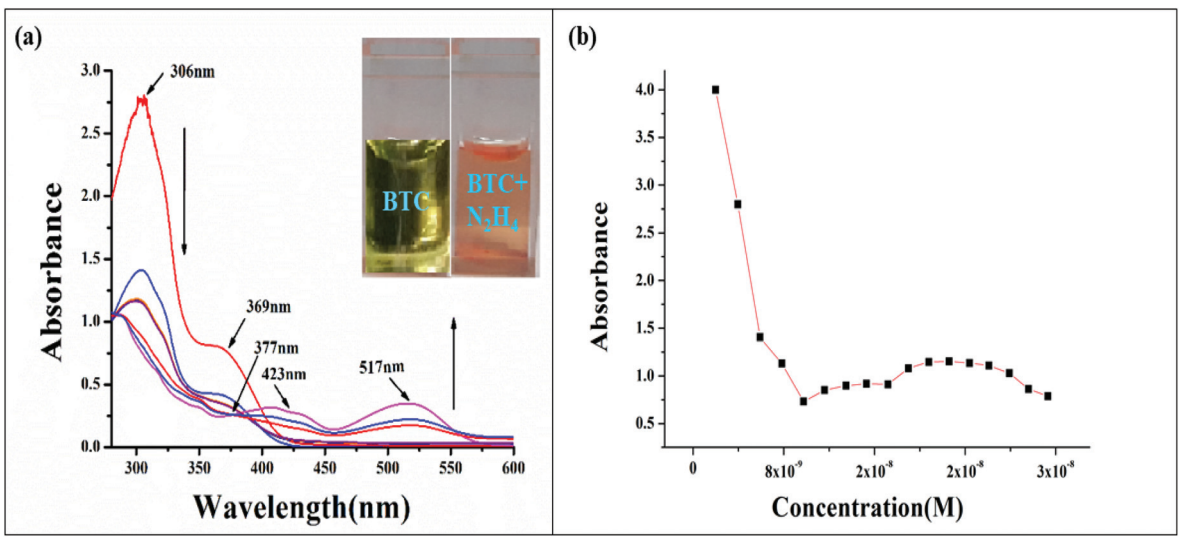

Fig. 1 (a) UV-vis absorption titration spectra of **BTC** ($c = 4 \times 10^{-5}$ M) in aq. DMSO (DMSO/H_2O = 7 : 3 v/v, 10 mM HEPES buffer, pH = 7.4) upon the addition of N_2H_4 ($c = 4 \times 10^{-4}$M). Inset: The photographs showed the color change of **BTC** in the presence of N_2H_4. (b) Absorbance change of **BTC** (40 μM) upon the addition of various concentrations of N_2H_4.

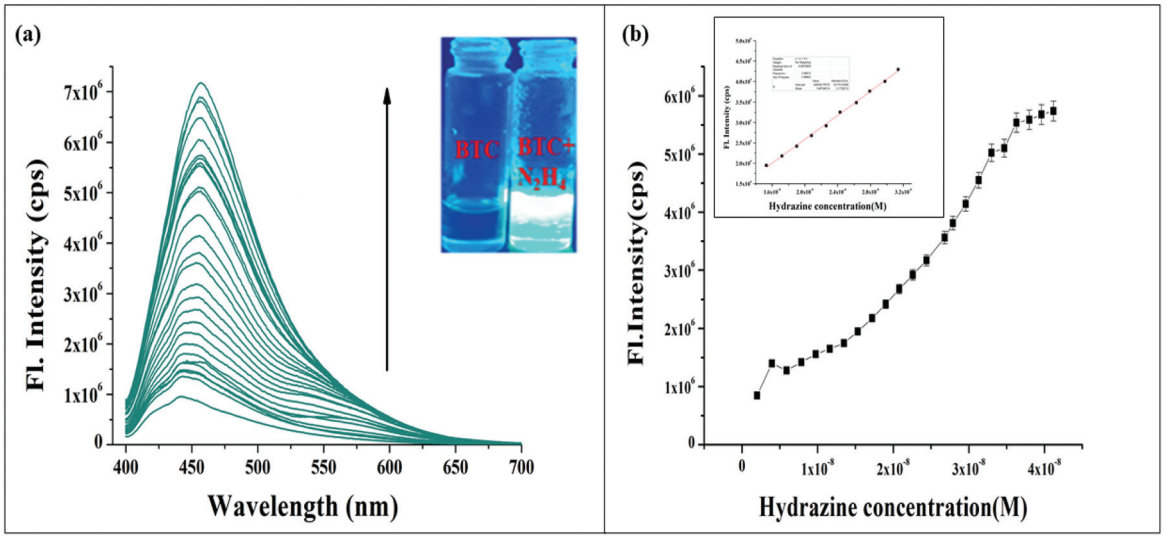

Fig. 2 (a) Fluorescence emission spectra obtained during the titration of **BTC** (c = 4 × 10^{-5} M) with N_2H_4 (c = 4 × 10^{-4} M) in aqueous DMSO (DMSO/H_2O = 7 : 3 v/v, 10 mM HEPES buffer, pH = 7.4), λ_{ex} = 390 nm. Inset: The fluorescence emission color changes of the probe **BTC** solution on the addition of hydrazine. (b) Fluorescence intensity changes (F_{446}) of **BTC** (40 μM) upon the addition of various concentrations of N_2H_4. Inset: The linear diagram of the probe **BTC** within the hydrazine concentration range.

maximum at 446 nm (λ_{ex} = 390 nm). However, the introduction of hydrazine solution elicited a gradual increase of emission intensities at 446 nm.

The significant enhancement of emission intensities (700-fold, quantum yield = 0.67) at 446 nm indicates after the chemical reaction of **BTC** with hydrazine the intramolecular charge transfer process (ICT) and the photoinduced electron transfer process (PET) which were operating between benzothiazole and methyldicyanovinyl coumarin suddenly become inhibited which was responsible for this fluorescence intensity enhancement. This result indicates the formation of the **BTC-A**$^-$ intermediate as well as the chemical transformation (Scheme 5). This result indicates the formation of a new species. The huge increase in the fluorescence intensity of **BTC** to N_2H_4 was also corroborated by the emission colour change of the solution from weakly fluorescent to highly intense sky blue upon the addition of N_2H_4 solution. Moreover, the fluorescence emission intensity gradually increases with an increase in the hydrazine concentration (Fig. 2b) as the gradual addition of hydrazine facilitated the lactone ring-opening reaction. The probe **BTC** exhibited a linear relationship in the range between 16 and 32 nM.

Solvent dependent fluorescence response of the probe BTC towards hydrazine detection

The solvent system influenced greatly the UV-vis and fluorescence spectrum. The optical property and sensing mechanism of the probe **BTC** with the analyte hydrazine was studied in a different solvent system. To investigate the solvent-dependent fluorescence change and UV spectral change, three types of solvent systems, *i.e.*, DMSO (polar aprotic solvent), MeOH (polar protic solvent), and $CHCl_3$, benzene, cyclohexane, *etc.* (nonpolar solvents), were basically chosen (Scheme 3). The nature of the absorbance spectra of the product **BTC-A** (Scheme 5) in the three solvents remained almost the same. But the fluorescence spectra of the product **BTC-A** in the three solvents were different (Fig. 3a). This phenomenon is known as solvatochromism (Scheme 4). In polar protic solvents like MeOH, two major emission peaks corresponding to strong enol emission (sky blue emission) at 446 nm and a weak keto emission (green emission) at 532 nm of the product **BTC-A** were observed (Fig. 3a). The strong enol emission peak was due to stabilization of the enol form in the polar protic solvent through intermolecular H-bonding interaction which inhibited tautomerization of the enol form to the keto form in the excited state. But upon the addition of H_2O to MeOH, the reverse phenomenon was observed, *i.e.*, the weak keto emission peak at 532 nm converted to strong keto emission with a simultaneous appearance of weak enol emission at 446 nm (Fig. 3a). The observed phenomenon was because, after the addition of water, water molecules formed intermolecular H-bonding with the polar protic solvent MeOH which diminished the stabilization of the enol form in MeOH *via* intermolecular H-bonding, facilitating tautomerization of the enol form to the keto form. Upon changing the solvent from polar protic solvents to nonpolar solvents like $CHCl_3$, cyclohexane, benzene, *etc.*, the enol emission peak at 446 nm vanished and a strong keto emission peak at 532 nm with a large Stokes shift was observed (Fig. 3a). The large Stokes shift was due to the transformation of the enol form to the keto form *via* intramolecular –OH proton transfer to the thiazole N atom through ESIPT, resulting in an increase in the conjugated chain length which indicated that the product **BTC-A** mainly existed in the keto form in a nonpolar solvent. Moreover, we also observed different Stokes shifts of the product **BTC-A** in different nonpolar solvents (Fig. 3a). The bathochromic shift of the keto form of the product **BTC-A** in cyclohexane was greater compared to

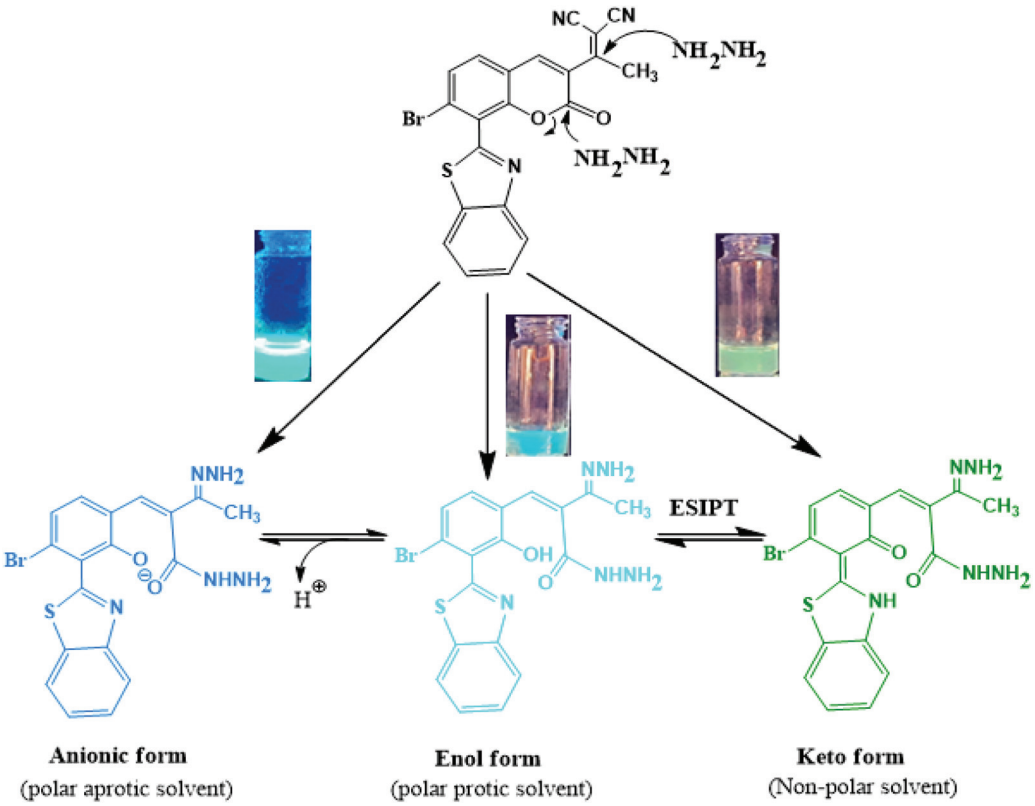

Scheme 3 Proposed sensing mechanism of the probe **BTC** in different solvents.

benzene and $CHCl_3$. This was probably due to different extents of stabilization of n–π* transition of the keto form of the product **BTC-A**. In polar aprotic solvents like DMSO and DMF, the situation was quite different. The basicity of these solvents was quite high to the abstract a proton of the product **BTC-A** which caused the formation of the deprotonated enol form.[52] Due to deprotonation, the ESIPT (excited-state intramolecular proton transfer) process and the PET (photoinduced electron transfer) process accompanied by the ICT (intramolecular charge transfer) process from benzothiazole to the electron-withdrawing methyldicyanovinyl coumarin moiety were inhibited resulting in significant fluorescence enhancement. As a result, a strong enolate emission peak with increased emission intensity at 446 nm was observed. Here, we chose DMSO as a solvent to investigate the fluorescence property of the product **BTC-A**. We also investigated the effect of water percentage on the emission of the product **BTC-A**. With an increase in water percentage, the percentage caused effective solvation of the hydrazine molecule reducing its reactivity and increasing the recognition time. So, we chose a suitable solvent ratio (DMSO/H_2O = 7 : 3 v/v) to perform the spectral change experiment. The UV-vis and fluorescence spectral change was recorded in aqueous DMSO (DMSO/H_2O = 7 : 3 v/v, 10 mM HEPES buffer, pH = 7.4) solution.

Selectivity and specificity of the probe BTC to hydrazine

To test the selectivity of the probe **BTC**, various analytes (10 equiv.), *i.e.*, (1) *n*-butyl amine, (2) NH_4OH, (3) CN^-, (4) triethylamine, (5) N_2H_4, (6) pyridine, (7) ethylenediamine, (8) HSO_3^-, (9) CH_3COO^-, (10) F^- and (11) ClO^- in DMSO–H_2O (10.0 mM HEPES buffer, 7 : 3 v/v, pH 7.4, at 25 °C), were added to the probe's solution (Fig. 4a). But no significant fluorescence change except for N_2H_4 was observed, which indicates that the probe is highly selective towards N_2H_4 over other analytes and this distinction was possible due to N_2H_4 induced lactone ring-opening (Fig. 4b).

Response time experiments of BTC

The time-dependent response of the probe **BTC** towards N_2H_4 was also studied. The fluorescence intensity changes of the probe **BTC** (40 μM) with varying concentrations of N_2H_4 from 0–700 μM was also studied over an incubation period of 0–100 s (Fig. 5). Time-dependent fluorescence response showed that the reaction of the probe **BTC** with N_2H_4 could be completed within seconds (Fig. 5). Moreover, the fluorescence intensity at 446 nm increased with increasing N_2H_4 concentration in the range between 400 and 700 μM; the higher the concentration of N_2H_4, the greater the signal-to-noise ratio and the faster the response. Also, the change was easily discernible to the naked eye under 390 nm irradiation.

From the kinetic study experiment, we obtained that the reaction of the probe **BTC** (40 μM) with N_2H_4 (400 μM) followed pseudo-first-order kinetics in aqueous DMSO (DMSO/H_2O = 7 : 3 v/v, 10 mM HEPES buffer, pH = 7.4) solution at room temperature. The pseudo-first-order rate constant (k_{obs})

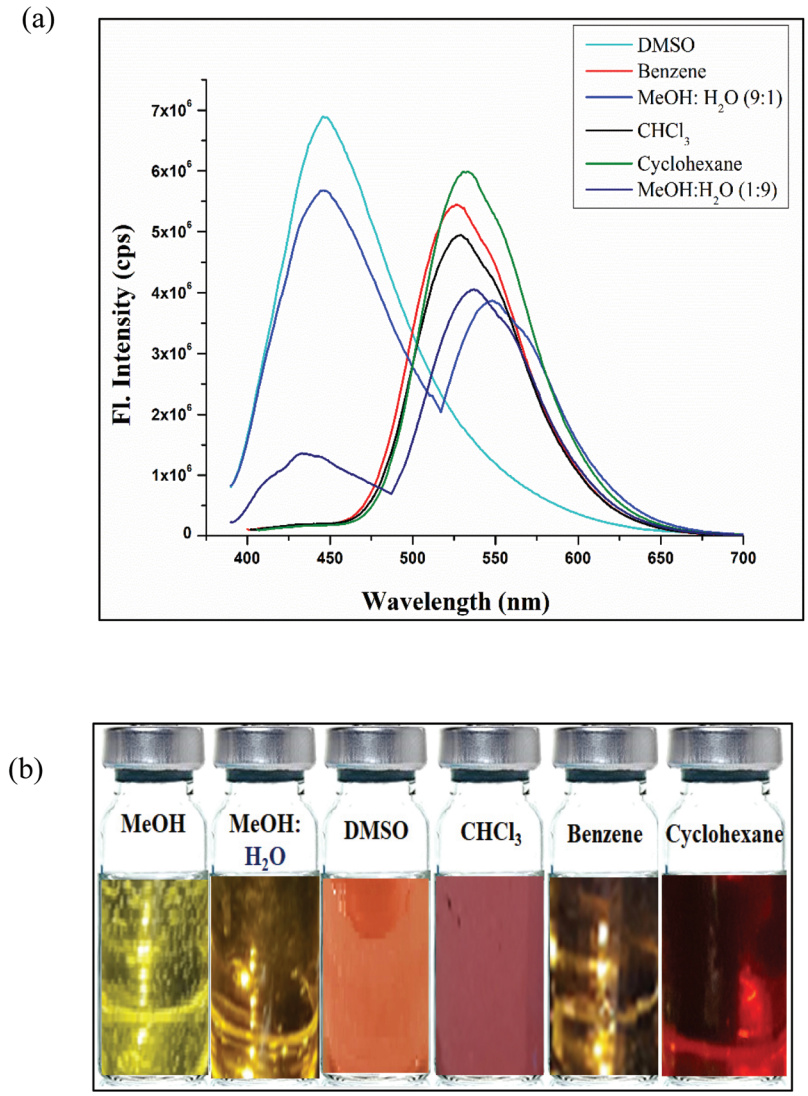

Fig. 3 (a) Fluorescence emission spectra of the probe **BTC** in different solvents under excitation at 390 nm. (b) Photographs of the probe **BTC** under a UV lamp (306 nm) in different organic solvents.

for the N_2H_4 induced lactone ring-opening was found to be k' = 0.013 s^{-1} (Fig. 7b). The observed rate constant k' was calculated according to eqn (1):

$$\ln(F_{max} - F_t)/F_{max} = -k't \quad (1)$$

where F_t and F_{max} are the fluorescence intensities at 446 nm at time t and the maximum value obtained after the completion of the reaction respectively and k' was the observed pseudo-first-order rate constant (Fig. S10, ESI†).

Computational method

For the determination of the electronic behavior of the probe and product, we performed quantum chemical DFT calculation by using the Gaussian 09 program with the assistance of the Gauss View visualization program. The probe and the product were optimized by using the B3LYP/6-311G+(d, p) basis set (Fig. 6). Consequently, for the understanding of the absorption properties of the probe, we performed the time-dependent density functional theory at an identical level. In excited-state computations, the solvent effect of DMSO was deemed *via* the polarizable continuum model (CPCM).

From the optimized geometries of the probe and product, it is found that initially the probe **BTC** is nonplanar because the benzothiazole moiety was perpendicular to the benzocoumarin ring making it less conjugated and weakly fluorescent. However, after NH_2NH_2 induced lactone ring-opening the *ortho* hydroxy proton which was blocked became free forcing the benzothiazole ring to become somehow tilted causing extended conjugation and a strong emission due to the inhibition of PET and ICT.

The calculated λ_{max} of the main orbital transition and oscillator strength (f) are given in Table S1 in the ESI.† The TD-DFT study revealed that the vertical major transitions

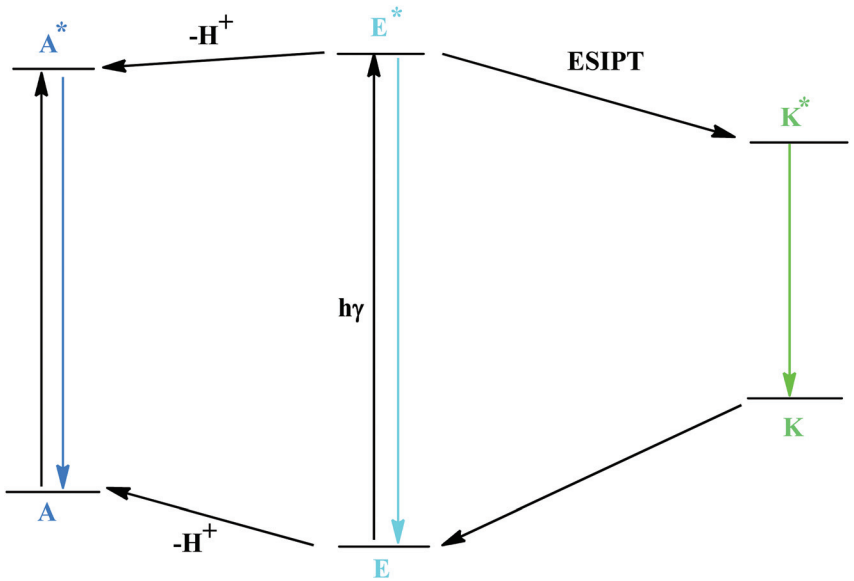

Scheme 4 Pictorial solvatochromism model of the probe **BTC**.

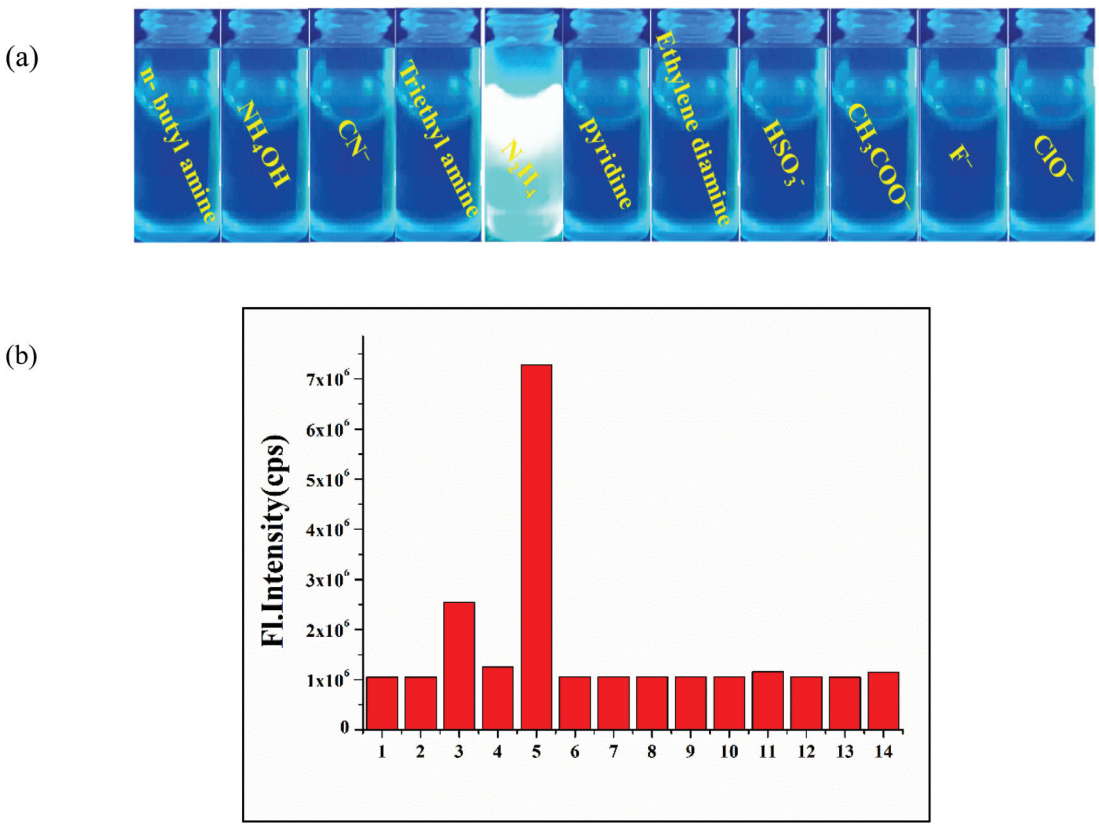

Fig. 4 (a) Fluorescence color changes of receptor **BTC** in aq. DMSO (DMSO : H_2O = 7 : 3 v/v, 10 mM HEPES buffer, pH = 7.4) upon the addition of various analytes (1) *n*-butyl amine, (2) NH_4OH, (3) CN^-, (4) triethylamine, (5) N_2H_4, (6) pyridine, (7) ethylenediamine, (8) HSO_3^-, (9) CH_3COO^-, (10) F^-, and (11) ClO^-. (b) Competitive fluorescence emission spectra of compound **BTC** in the presence of different analytes in aq. DMSO (DMSO/H_2O = 7 : 3).

observed at about 379 nm are comparable to those of the experimentally observed spectra at about 390 nm for the probe. The calculated band at 379 nm is assigned to the HOMO–LUMO transition with the observed oscillator strength (f = 0.0026) corresponding to the experimental λ_{max} (~390 nm) (ESI, Table S1†). Finally, we can say that theoretical UV-vis

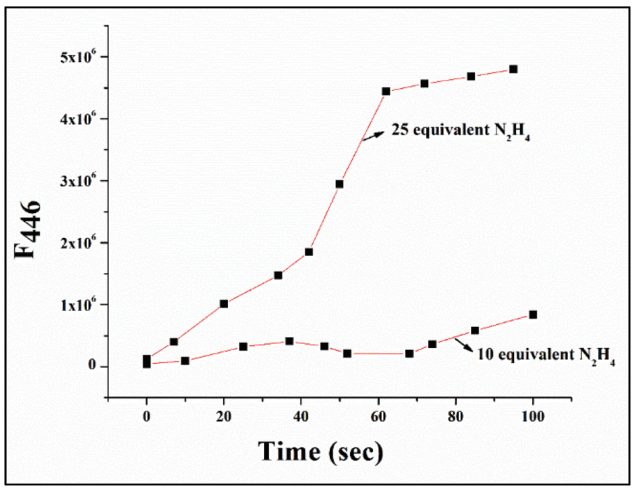

Fig. 5 Time course (0–100 s) of fluorescence enhancement of **BTC** (40 μM) in DMSO solution upon the addition of two concentrations (10 equiv. and 25 equiv.) of N_2H_4 λ_{ex} = 390 nm; λ_{em} = 446 nm.

spectra calculated by TDDFT agreed well with the experimental observations.

In the probe **BTC** both the HOMO and LUMO are localized on different skeletons, *i.e.*, in the benzothiazole and benzocoumarin moiety. But in **BTC-A**$^-$ both HOMO and LUMO are localized in the same benzocoumarin moiety. As a result, the energy difference between HOMO and LUMO of adduct **BTC-A**$^-$ is lower compared to the probe **BTC** which supports a bathochromic shift.

Temperature effect

To investigate temperature-dependent fluorescence study the sample solution of the probe **BTC** was cooled below room temperature by placing it into the low-temperature bath. The relative magnitude of the fluorescence signal intensity varied with temperature as lactone ring-opening was highly dependent on temperature. With the rise of temperature, the intensity of the fluorescence signal was also increased (Fig. 8). The above phenomenon can also be explained by taking into account thermodynamic consideration. According to Gibb's equation we know, $\Delta G = \Delta H - T\Delta S$. Due to the hydrazine-induced lactone ring-opening reaction a highly conjugated stable product was formed. During the lactone ring-opening reaction ΔH is highly −ve, ΔS is highly +ve as the translational and rotational degree of freedom of the cyclic ring is highly relaxed in its open conjugated form. To make feasible the ring-opening reaction, ΔT should be +ve. With the rise in temperature from 25 °C to 35 °C, the fluorescence intensity signal also increased.

The observed phenomenon was because after the hydrazine-induced lactone ring-opening reaction, the enol form of the product **BTC-A** became easily converted to the enolate form through deprotonation or cleavage of the O–H bond which inhibited the PET (photoinduced electron transfer) and ICT (intramolecular charge transfer) process operating between the benzothiazole and methyldicyanovinyl coumarin moiety of the probe **BTC** resulting in a significant increase of the fluorescence intensity signal.

Effect of pH

The pH-dependent fluorescence change of the probe **BTC** was also studied. To do this experiment a set of buffer solutions ranging from pH 1 to pH 12 were also prepared and pH titration of the probe **BTC** was carried out in the absence or presence of hydrazine. It was observed that the fluorescence intensity of the probe **BTC** gradually increased from pH 1 to pH 5

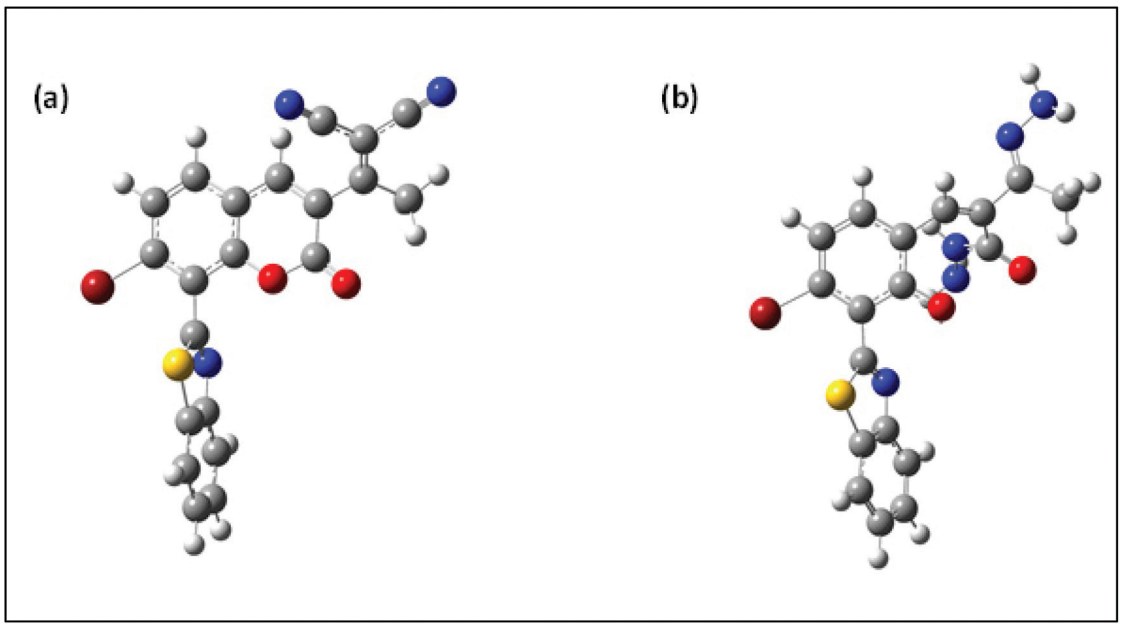

Fig. 6 Optimized structure of the (a) probe **BTC** and (b) product **BTC-A**$^-$ using the B3LYP/6-311G+(d,p).

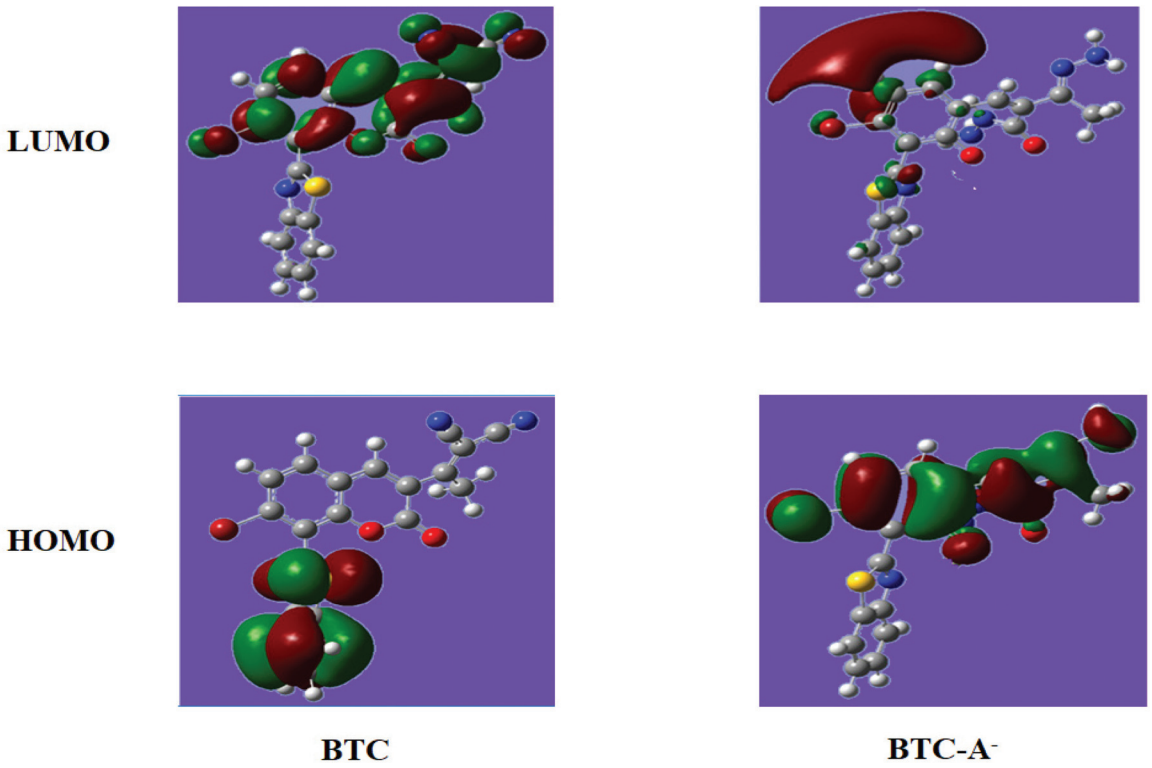

Fig. 7 HOMO and LUMO distributions of the probe **BTC** and product **BTC-A**$^{-}$.

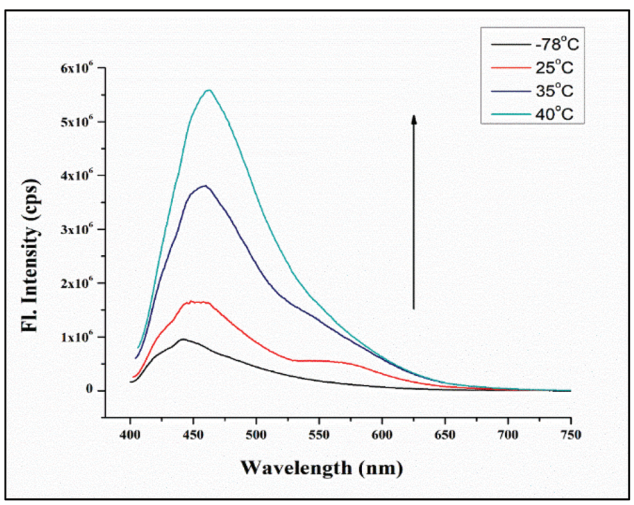

Fig. 8 Fluorescence emission intensity of the probe **BTC** in DMSO (40 μM) at different temperatures.

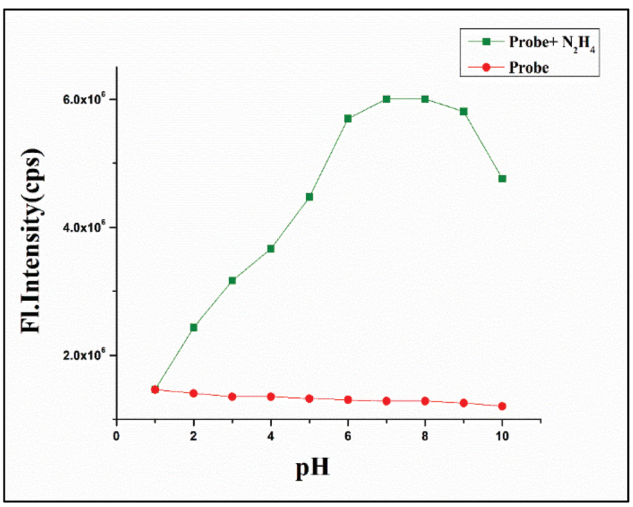

Fig. 9 pH-Dependent changes in the fluorescence intensity of the probe **BTC** (1×10^{-5} M) in the absence or presence of hydrazine (1×10^{-4} M) in DMSO–H_2O (DMSO/H_2O = 7 : 3 v/v, 10 mM HEPES buffer, pH = 7.4). So, from the fluorescence intensity *vs.* pH graph it has been seen that the fluorescence intensity of the probe is maximum near about pH = 7.

and after pH 5 up to pH 8 a sharp increase in the fluorescence intensity was noticed and then after pH 8, the fluorescence intensity was somehow quenched (Fig. 9).

The observed phenomenon was due to the nucleophilicity of hydrazine being greatly affected in different pH regions. A gradual increase in the fluorescence intensity was observed up to pH 8 and then after pH 8 the fluorescence intensity decreased. In an extremely low pH region, *i.e.*, pH 1 or pH 2, the hydrazine molecule becomes protonated to observe any fluorescence and then up to pH 5, the fluorescence intensity values gradually increased as the electrophilicity of lactone ring gradually enhanced to facilitate the nucleophilic attack of hydrazine to open the lactone ring. After pH 5 the sharp

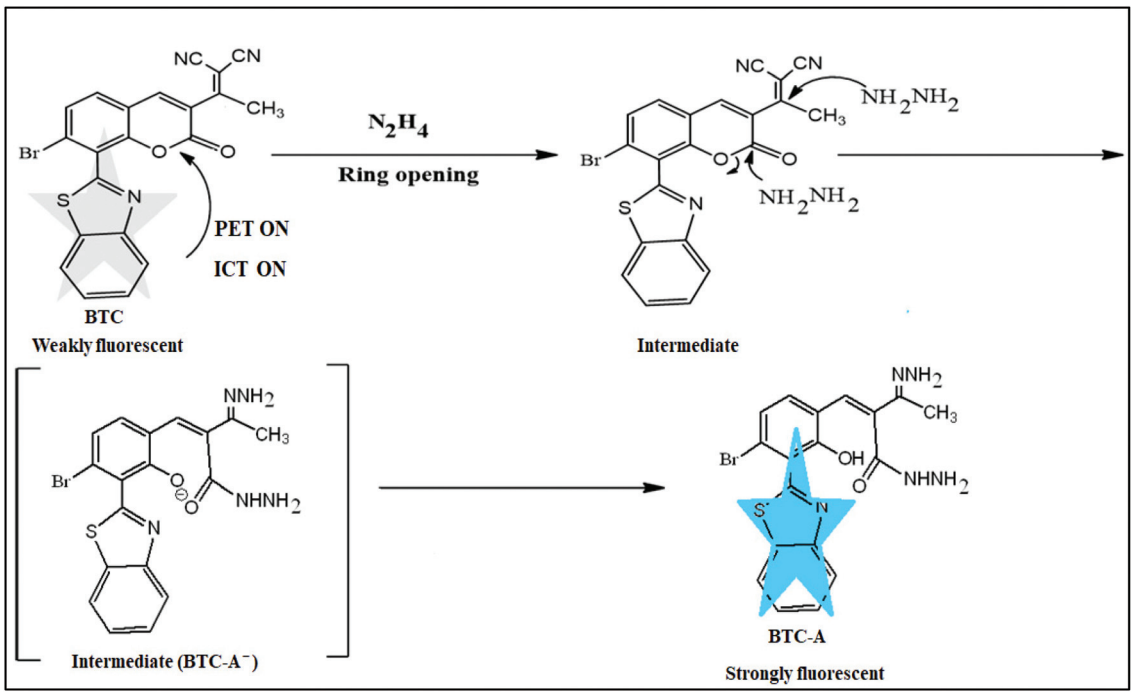

Scheme 5 Proposed hydrazinolysis mechanism of the probe **BTC** to hydrazine.

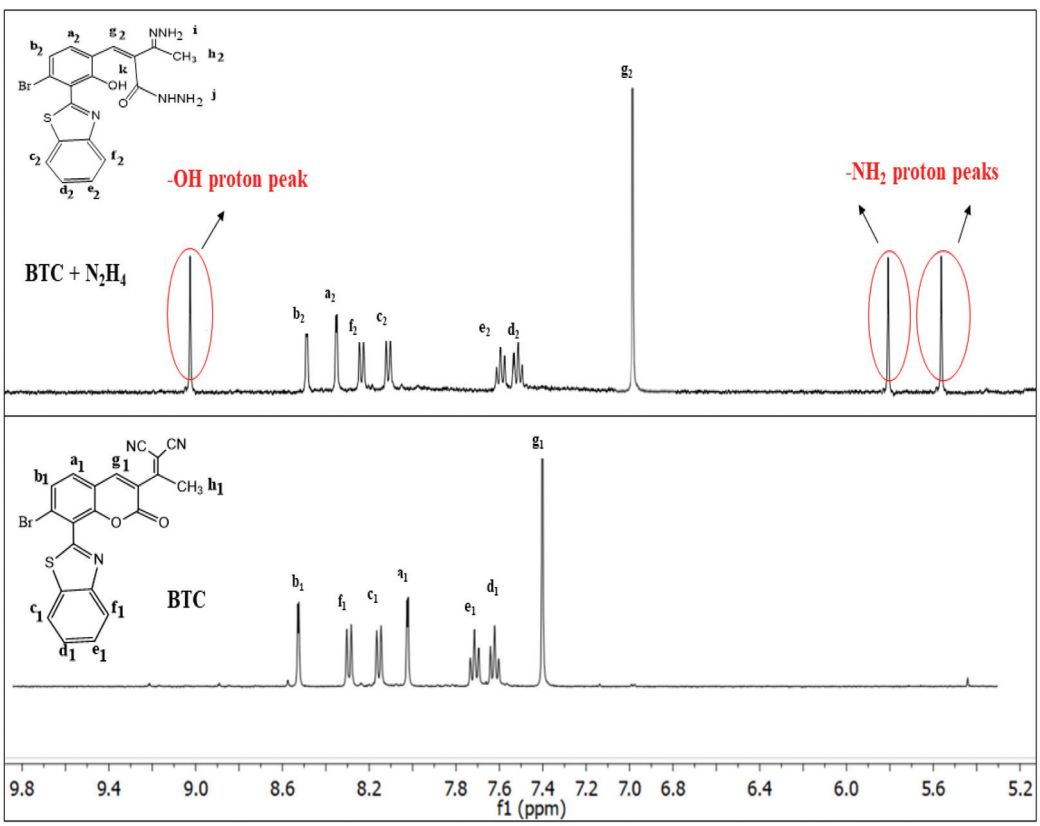

Fig. 10 ^{1}H NMR titration of the probe **BTC** with hydrazine.

increase in the fluorescence intensity was noticed because in this region the nucleophilicity of hydrazine and electrophilicity of the lactone ring both remained under extreme conditions resulting in a significant naked eye sharp fluorescence intensity increase of the signal. Then after pH 8, the fluorescence of the probe **BTC** was again quenched. Hence the probe **BTC** was sufficiently stable in pH regions 5 to 8. Beyond this pH region, *i.e.*, below pH 5 (strongly acidic condition) and above pH 8 (strongly alkaline condition), the probe **BTC** was unstable. Under strongly acidic conditions the probe **BTC** existed in the protonated form and under strongly basic conditions the probe **BTC** was unstable due to hydrolysis. The change of absorbance of the probe **BTC** with pH in the presence of hydrazine was also investigated. With the increase of pH from 1.0 to 4.0, the absorbance of the probe **BTC** gradually decreased, then a sharp decrease in absorbance was observed at pH 5.0. This decrease of pH was continued up to pH 7.0 and after that a slight increase in absorbance was noticed at pH 8.0 and then absorbance again decreased up to pH 10.0 (Fig. S7, ESI†). The sharp decrease in absorbance at pH 5.0 was due to hydrazine induced lactone ring opening which decreased the area of absorption. Then a slight increase in absorbance at pH 8.0 may be by a virtue of deprotonation and then at higher pH, the probe **BTC** was sufficiently unstable to observe a decrease in absorbance. From the above experiment, it was proved that the probe **BTC** could be used under physiological conditions.

Proposed detection mechanism

On the basis of the fluorescence spectra of the probe **BTC** the proposed sensing mechanism of the probe **BTC** towards hydrazine is shown in Scheme 5. At first hydrazine attacks the electron deficient lactone ring and then subsequently the dicyano-

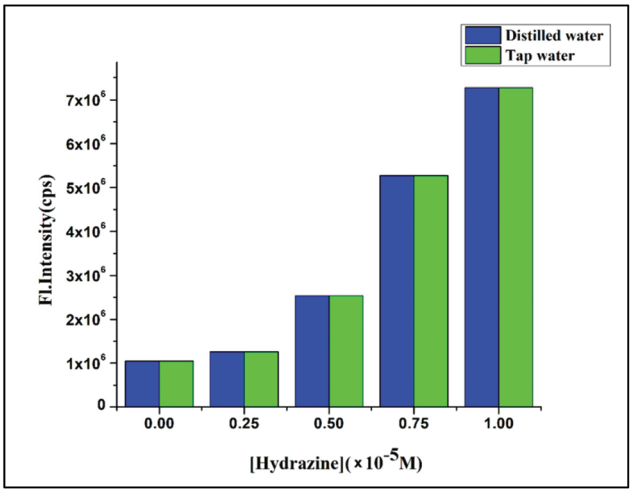

Fig. 12 Competitive fluorescence intensity changes of the probe **BTC** in distilled water and tap water.

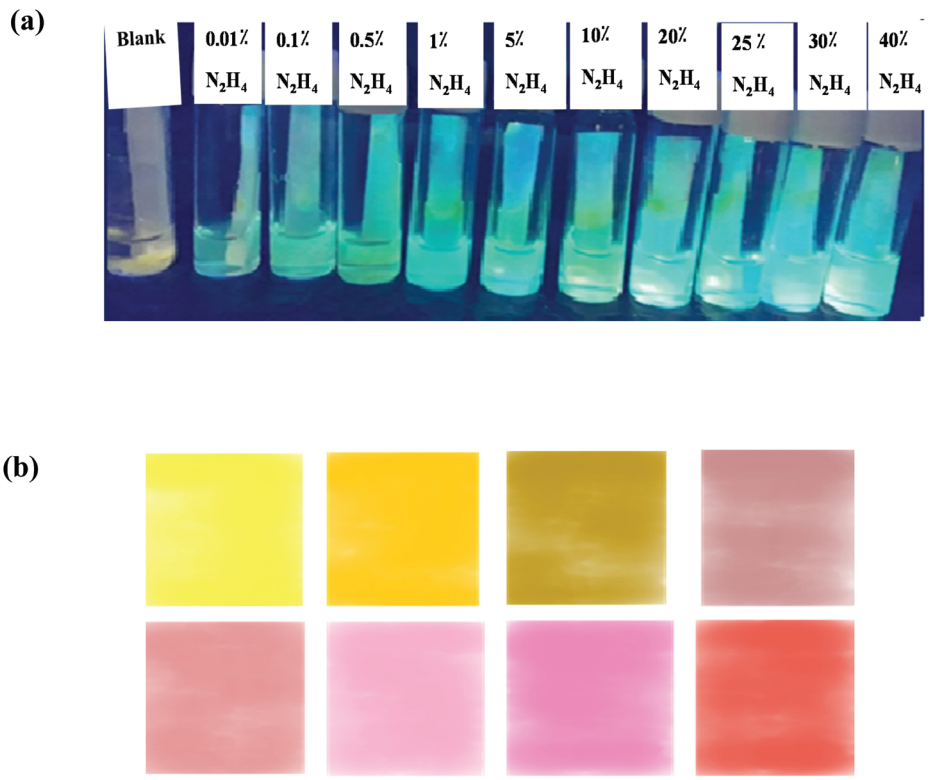

Fig. 11 (a) Fluorescence color changes of the probe **BTC** (5.0 mM) coated filter paper after exposure to different concentrations (blank, 0.1%, 0.5%, 1%, 5%, 10%, 20%, 25%, 30%, 40% and 50%) of hydrazine in aqueous solution. (b) Naked eye color changes of the probe **BTC** (5.0 mM) coated filter paper after exposure to different concentrations of hydrazine.

vinyl group cleavage to generate the product **BTC-A**. Due to the formation of the product **BTC-A** a remarkable fluorescence color change from colorless to intense sky blue was observed.

We have also designed a reference compound **R1** where the methyl dicyanovinyl group is absent in the lactone ring (Scheme 2 and Fig. S12†). But in the presence of hydrazine the reference compound **R1** did not show any significant change in the fluorescence intensity signal. This was due to the presence of the Br atom which is fluorescence quencher and lack of extended conjugation compared to the probe **BTC**. This proved that the probe **BTC** was superior compared to reference compound **R1**.

The proposed sensing mechanism of the probe **BTC** towards hydrazine (Fig. 10) was evidenced by the ^{1}H NMR titration and ESI-MS spectrum experiment. The ^{1}H NMR experiment showed that the peak position of protons, *i.e.* a_1, b_1, c_1, d_1, e_1, f_1, and g_1, shifted upfield (forward) to a_2, b_2, c_2, d_2, e_2, f_2 and g_2, respectively with the appearance of three new peaks corresponding to hydroxyl proton (δ = 10.5 ppm) and amino protons (δ = 5.5 and 6.0 ppm) after reaction with hydrazine (Fig. 10). The above result proved that hydrazine induced the lactone ring-opening reaction upon the addition of hydrazine. The formation of adduct **BTC-A** was also proved by ESI-MS spectrum analysis, calc. for $C_{18}H_{16}BrN_5O_2S$ [**BTC** + hydrazine]$^+$ 445.0208, found: 445.0206 (Fig. S11, ESI†).

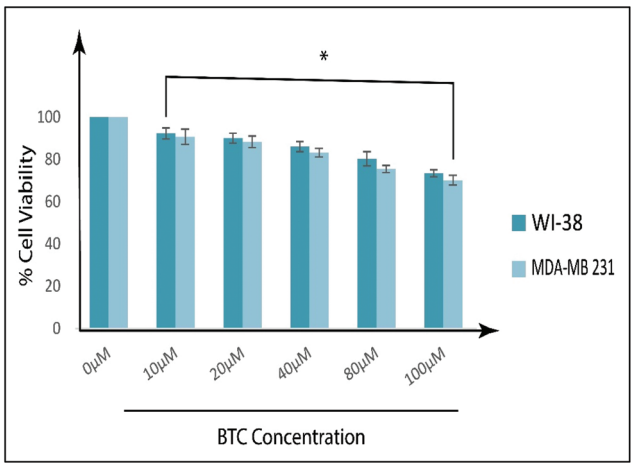

Fig. 13 Cell survivability of MDA-MB 231 and WI-38 cells exposed to different probe **BTC** concentrations. Data are representative of at least three independent experiments and bar graph shows mean ± SEM, *p < 0.001 was interpreted as statistically significant, as compared with the control.

Vapor phase hydrazine detection

To investigate the practical application of the probe **BTC**, test strips were prepared by immersing filter paper in the aqueous DMSO (3/7, v/v) mixture at pH 7.4 solutions of **BTC** (1.0×10^{-2} M) and then dried in air. The test strips containing **BTC** were utilized to sense hydrazine. As shown in Fig. 11b, when hydrazine was added to the test kits at various concentrations (1.0×10^{-5} M, 1.0×10^{-4} M, 1.0×10^{-3} M, 1.0×10^{-2} M, 4.0×10^{-2} M) the naked eye color change from light yellow to reddish brown under the 390 nm UV-lamp were observed. Therefore, the test

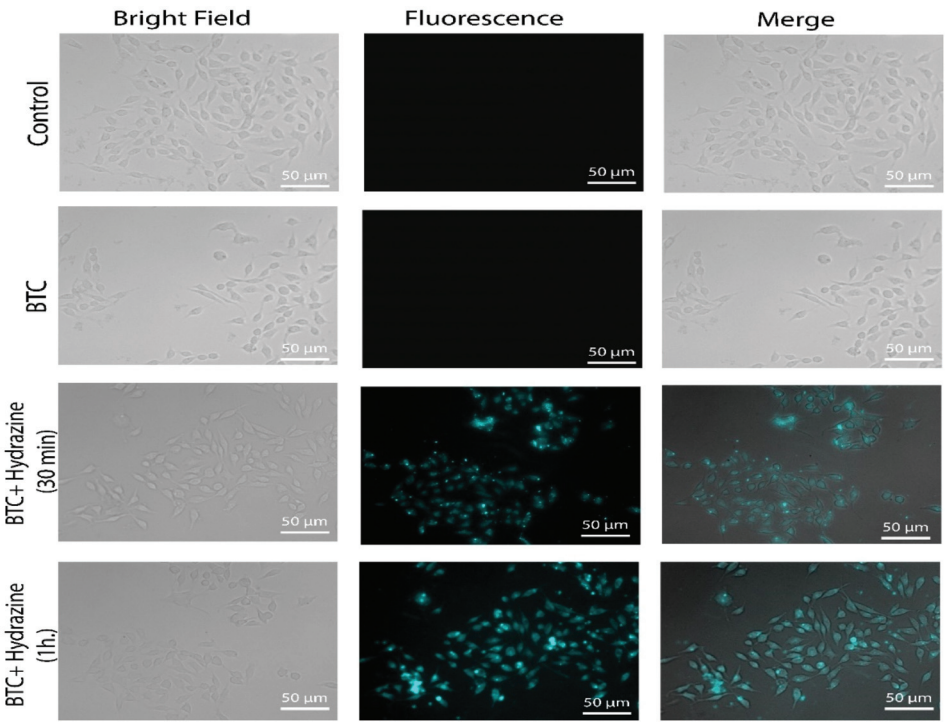

Fig. 14 Microscopic images of untreated MDA-MB 231 cells (control), cells treated with the probe **BTC** (15 μM), the probe **BTC** (15 μM) + hydrazine (10 μM) together after 30 min and 1 h, incubation period under bright, fluorescence and merged field.

strips coated with the **BTC** probe solution would be convenient for detecting hydrazine. These results showed that the probe **BTC** could have a practical application for detecting hydrazine in water samples. To make the detection experiments easy to perform and practical, test strips were used. Prior to detection, test strips were prepared by sinking the filter paper with the probe **BTC** (5.0 mM) in aqueous DMSO (3/7, v/v) solution and then dried. The probe loaded test strips were covered on the top of jars that contained different hydrazine solution concentrations (blank, 0.1%, 0.5%, 1%, 5%, 10%, 20%, 25%, 30%, 40%, and 50% in water) for 30 min at room temperature before it was ready to observe. The fluorescence color of the strips gradually became intense from light green to intense bright sky blue, which proved that the fluorescence intensity of the probe on the test strips was highly dependent on the concentration of hydrazine in aqueous solution and easy to distinguish with the naked eye (Fig. 11a).

Hydrazine detection in real water samples

We also studied the practical application of the probe **BTC** for the detection of hydrazine in different water samples. Hydrazine is an important chemical reagent used in the chemical and pharmaceutical industries there is a possibility of mixing this hazardous waste into water. For this reason, the detection of hydrazine is also important in different water samples. A little amount of hydrazine was added to different water samples, *i.e.*, tap water and distilled water. In the presence of **BTC**, the fluorescence intensity signals were compared in tap water and distilled water (Fig. 12). The probe **BTC** can detect hydrazine in both water samples up to 1.7 nM. The results proved that the probe **BTC** could detect hydrazine quantitatively in real water samples.

Biological cell-imaging of hydrazine

In vivo cell cytotoxicity assay of the probe **BTC** was checked on MDA-MB 231 and WI-38 cell lines. Data from MTT assay showed no substantial toxicities even at the concentration of 100 μM of the probe **BTC** (Fig. 13). Hence, 15 μM working concentration of the probe **BTC** was selected to perform further studies.

Results from fluorescence microscopy imaging showed an increased level of fluorescence intensity at an emission level of 446 nm when MDA-MB 231 cells were exposed to the probe **BTC** (15 μM) in combination with hydrazine (10 μM) at an incubation time frame of 30 min and 1 h, compared to untreated as well as cells treated with only the probe **BTC** (Fig. 14) that showed no fluorescence. Thus, we can conclude that the probe **BTC** detects hydrazine and results in sky blue fluorescent luminescence. Hence, our synthesized probe **BTC** is biocompatible and favourable for biological applications.

Conclusion

In this paper, we have designed and synthesized a probe **BTC** for the selective detection of hydrazine in water samples and in living cells based on the hydrazine-induced lactone ring-opening reaction. The presence of –Br and methyldicyanovinyl in the probe **BTC** made the lactone ring highly electron-deficient to facilitate the nucleophilic attack of highly electron-rich hydrazine for the lactone ring-opening reaction and the lactone ring-opening reaction caused a large Stokes shift and a high fluorescence quantum yield. As a result, strong sky-blue fluorescence "turn-on" was observed from the "turn-off" state which proved the probe's high selectivity and sensitivity compared to other anions and analytes. The selectivity and sensitivity of the probe **BTC** were evidenced by fluorescence, absorption, ESI mass spectrometry, ^{1}H NMR spectroscopy, and visual fluorescence colour changes. Moreover, compared to previously reported fluorescent probes, our probe **BTC** can detect hydrazine rapidly and with a very low detection limit. Finally, the probe **BTC** was successfully applied for the detection of hydrazine in the vapour phase, real water samples, and live cells.

Conflicts of interest

The authors declare no conflict of interest for this manuscript.

Acknowledgements

AM gratefully acknowledges CSIR, New Delhi [File No.: 08/003 (0139)/2019-EMR-I] for the fellowship. DB thanks CSIR, New Delhi [File No.: 08/003(0143)/2020-EMR-I] for the fellowship.

References

1 J. O. Edwards and R. G. Pearson, *J. Am. Chem. Soc.*, 1962, **84**, 16–24.
2 U. Ragnarsson, *Chem. Soc. Rev.*, 2001, **30**, 205–213.
3 S. Garrod, M. E. Bollard, A. W. Nicholls, S. C. Connor, J. Connelly, J. K. Nicholson and E. Holmes, *Chem. Res. Toxicol.*, 2005, **18**, 115–122.
4 S. S. Narayanan and F. Scholz, *Electroanalysis*, 1999, **11**, 465–469.
5 K. Yamada, K. Yasuda, N. Fujiwara, Z. Siroma, H. Tanaka, Y. Miyazaki and T. Kobayashi, *Electrochem. Commun.*, 2003, **5**, 892–896.
6 J. I. Kroschwitz and A. Seidel, Hydrazine and Its Derivatives, in *Kirk-Othmer Encyclopedia of Chemical Technology*, Wiley, New York, 5th edn, 2005, vol. 13, pp. 562–607.
7 E. H. Vernot, J. D. MacEwen and R. H. Bruner, *Fundam. Appl. Toxicol.*, 1985, **5**, 1050.
8 C. A. Reilly and S. D. Aust, *Chem. Res. Toxicol.*, 1997, **10**, 328–334.
9 K. MDJ and T. JA, *Compr. Toxicol.*, 1997, **120**, 221–230.
10 U.S. Environmental Protection Agency (EPA), *Integrated Risk Information System (IRIS) on Hydrazine/Hydrazine Sulfate*, National Centerfor Environmental Assessment, Office of Research and Development, Washington, DC, 1999.
11 G. Collins and S. R. Pehrsson, *Analyst*, 1994, **119**, 1907.

12 D. Elder, D. Snodin and A. Teasdale, *J. Pharm. Biomed. Anal.*, 2011, **54**, 900–910.
13 H. Malone, *Anal. Chem.*, 1961, **33**, 575–577.
14 X. Gu and J. Camden, *Anal. Chem.*, 2015, **87**, 6460–6464.
15 A. Umar, M. M. Rahman, S. H. Kim and Y.-B. Hahn, *Chem. Commun.*, 2008, 166–168.
16 A. P. Demchenko, *Introduction to Fluorescence Sensing*, Springer, New York, 2008.
17 Y. Sun, D. Zhao, S. Fan and L. Duan, *Sens. Actuators, B*, 2015, **208**, 512–517.
18 D.-Y. Qu, J.-L. Chen and B. Di, *Anal. Methods*, 2014, **6**, 4705–4709.
19 K. Li, H.-R. Xu, K.-K. Yu, J.-T. Hou and X.-Q. Yu, *Anal. Methods*, 2013, **5**, 2653–2656.
20 H. Tse, Q. Li, S. Chan, Q. You, A. W. M. Lee and W. Chan, *RSC Adv.*, 2016, **6**, 14678–14681.
21 C. Hu, W. Sun, J. Cao, P. Gao, J. Wang, J. Fan, F. Song, S. Sun and X. Peng, *Org. Lett.*, 2013, **15**, 4022–4025.
22 J. Zhang, L. Ning, J. Liu, J. Wang, B. Yu, X. Liu, X. Yao, Z. Zhang and H. Zhang, *Anal. Chem.*, 2015, **87**, 9101–9107.
23 L. Cui, Z. Peng, C. Ji, J. Huang, D. Huang, J. Ma, S. Zhang, X. Qian and Y. Xu, *Chem. Commun.*, 2014, **50**, 1485–1487.
24 R. Maji, A. K. Mahapatra, K. Maiti, S. Mondal, S. S. Ali, P. Sahoo, S. Mandal, Md. R. Uddin, S. Goswami, C. K. Quah and H. K. Fun, *RSC Adv.*, 2016, **6**, 70855–70862.
25 F. Ali, H. A. Anila, N. Taye, D. G. Mogare, S. Chattopadhyay and A. Das, *Chem. Commun.*, 2016, **52**, 6166–6169.
26 L. Wang, F.-Y. Liu, H.-Y. Liu, Y.-S. Dong, T.-Q. Liu, J.-F. Liu, Y.-W. Yao and X.-J. Wan, *Sens. Actuators, B*, 2016, **229**, 441–452.
27 M. V. R. Raju, E. C. Prakash, H.-C. Chang and H.-C. Lin, *Dyes Pigm.*, 2014, **103**, 9–20.
28 Z. Ju, D. Li, D. Zhang, D. Li, C. Wu and Z. Xu, *J. Fluoresc.*, 2017, **27**, 679–687.
29 M. G. Choi, J. Hwang, J. O. Moon, J. Sung and S.-K. Chang, *Org. Lett.*, 2011, **13**, 5260–5263.
30 S. Yu, S. Wang, H. Yu, Y. Fenga, S. Zhang, M. Zhu, H. Yin and X. Meng, *Sens. Actuators, B*, 2015, **220**, 1338–1345.
31 A. K. Mahapatra, R. Maji, K. Maiti, S. K. Manna, S. Mondal, S. S. Ali, S. Manna, P. Sahoo, S. Mandal, M. R. Uddin and D. Mandal, *RSC Adv.*, 2015, **5**, 58228–58236.
32 S. Goswami, S. Das, K. Aich, D. Sarkar and T. K. Mondal, *Tetrahedron Lett.*, 2014, **55**, 2695–2699.
33 S. Goswami, A. K. Das, U. Saha, S. Maity, K. Khanra and N. Bhattacharyya, *Org. Biomol. Chem.*, 2015, **13**, 2134–2139.
34 B. Roy, S. Halder, A. Guha and S. Bandyopadhyay, *Anal. Chem.*, 2017, **89**, 10625–10636.
35 W.-N. Wu, H. Wu, Y. Wang, X.-J. Mao, X.-L. Zhao, Z.-Q. Xu, Y.-C. Fan and Z.-H. Xu, *Spectrochim. Acta, Part A*, 2018, **188**, 80–84.
36 S. Goswami, S. Paul and A. Manna, *RSC Adv.*, 2013, **3**, 18872–18877.
37 X. Yang, Y. Liu, Y. Wu, X. Ren, D. Zhang and Y. Yea, *Sens. Actuators, B*, 2017, **253**, 488–494.
38 M. Sun, J. Guo, Q. Yang, N. Xiao and Y. Li, *J. Mater. Chem. B*, 2014, **2**, 1846–1851.
39 B. Chen, X. Sun, X. Li, H. Ågren and Y. Xie, *Sens. Actuators, B*, 2014, **199**, 93–100.
40 Z. Li, W. Zhang, C. Liu, M. Yu, H. Zhang, L. Guo and L. Wei, *Sens. Actuators, B*, 2017, **241**, 665–671.
41 M. Sun, J. Guo, Q. Yang, N. Xiao and Y. Li, *J. Mater. Chem. B*, 2014, **2**, 1846–1851.
42 Z. Li, W. Zhang, C. Liu, M. Yu, H. Zhang, L. Guo and L. Wei, *Sens. Actuators, B*, 2017, **241**, 665–671.
43 J. Fan, W. Sun, M. Hu, J. Cao, G. Cheng, H. Dong, K. Song, Y. Liu, S. Sun and X. Peng, *Chem. Commun.*, 2012, **48**, 8117–8119.
44 G. H. Aryal, K. Lu, G. Chen, K. W. Hunter and L. Huang, *Chem. Commun.*, 2019, **55**, 13912–13915.
45 L. He, B. Dong, Y. Liu and W. Lin, *Chem. Soc. Rev.*, 2016, **45**, 6449–6461.
46 A. Pal, M. Karmakar, S. R. Bhatta and A. Thakur, *Coord. Chem. Rev.*, 2021, **448**, 214167.
47 P. R. Twentyman and M. Luscombe, *Br. J. Cancer*, 1987, **56**, 279–285.
48 M. Mandal, D. Sain, Md. M. Islam, D. Banik, M. Periyasamy, S. Mandal, A. Kar and A. K. Mahapatra, *Anal. Methods*, 2021, **13**, 3922–3929.
49 S. S. Ali, A. Gangopadhyay, A. K. Pramanik, U. N. Guria, S. K. Samanta and A. K. Mahapatra, *Dyes Pigm.*, 2019, **170**, 107585–107588.
50 U. N. Guria, A. Gangopadhyay, S. S. Ali, K. Maiti, S. K. Samanta, S. Manna, A. K. Ghosh, Md. R. Uddin, S. Mandal and A. K. Mahapatra, *Anal. Methods*, 2019, **11**, 5447–5454.
51 Y. Yang, Y. Feng, Y. Jiang, F. Qiu, Y. Wang, X. Song, X. Tang, G. Zhang and W. Liu, *Talanta*, 2019, **197**, 122–129.
52 K. Sakai, T. Ishikawa and T. Akutagawa, *J. Mater. Chem. C*, 2013, **1**, 7866–7871.